AIAA JOURNAL
Vol. 38, No. 6, June 2000

Planar Doppler Velocimetry in a Large-Scale Facility

A. D. Mosedale* and G. S. Elliott†
Rutgers University, Piscataway, New Jersey 08854
C. D. Carter‡
Innovative Scientific Solutions, Inc., Dayton, Ohio 45440
and
T. J. Beutner§
U.S. Air Force Research Laboratory, Wright–Patterson Air Force Base, Ohio 45433

A planar Doppler velocimetry (PDV) system was developed and demonstrated in a small-scale facility (Mach 1.36 freejet) and then applied in a large-scale subsonic wind tunnel, where measurements were made over a delta wing at a 23-deg angle of attack. This PDV system utilized a pulsed, injection-seeded, frequency-doubled Nd:YAG laser to interrogate the flow. Back-illuminated charge-coupled device (CCD) cameras in conjunction with an iodine filter were used to record images produced by the scattered laser light, permitting the determination of the velocity at each CCD pixel. The PDV instrument also included custom software and a frequency-monitoring system composed of photodiodes, gated integrators, and a second iodine cell. With this setup, we recorded the shot-to-shot iodine-filtered and reference images and the associated laser frequency. In the freejet, mean velocities in the core were measured by PDV to within 6.4 m/s (out of ~ 260 m/s) of the value obtained by laser Doppler velocimetry. In the wind tunnel, freestream empty-tunnel measurements indicated bias and random errors of less than 2 and 4 m/s, respectively. The dominant source of random error arose from laser speckle, and the dominant source of bias error came from the characterization of the iodine filters. Measurements over the delta wing showed similar velocity ranges but smaller vortex cores when compared to the velocity field predicted by a computational fluid dynamics model.

Introduction

PLANAR Doppler velocimetry (PDV) is a relatively new means of investigating the velocity field of gaseous flows. The method relies on a determination of the Doppler shift associated with light scattered from particles seeded into the flowfield and employs planar illumination of the probe region with light from a narrow-linewidth laser. The light scattered from the flowfield particles is then recorded with a digital array detector, and the Doppler shift is derived at each pixel. There are several reasons for interest in this technique. First, it can provide a means for rapidly surveying three-dimensional flowfields. This is an attractive feature in facilities where runtime is expensive. Second, simultaneous detection in three scattering directions yields three independent Doppler shifts, and therefore, three velocity components can be measured simultaneously. Third, because it is a planar technique, it can be used to investigate the formation of flow structures. Fourth, it promises to be feasible in large-scale facilities, where other nonintrusive techniques such as particle image velocimetry and laser Doppler velocimetry (LDV) become more difficult to apply.

PDV produces a quantitative velocity image of the plane of interest according to the following mechanism. For each pixel in the camera field of view, the local velocity is related to the Doppler shift according to the relation[1]

$$\Delta f_{\text{Doppler}} = [2\sin(\phi/2)/\lambda]V\cos(\Omega) \tag{1}$$

where $\Delta f_{\text{Doppler}}$ is the Doppler shift, λ is the wavelength of the incident laser light, ϕ is the angle between the incident and scattering vectors, and Ω is the angle between the velocity vector and the direction of PDV system sensitivity. This direction of sensitivity is the same as that of the vector difference between the scattering and incident vectors. V is the velocity magnitude, and $V\cos(\Omega)$ is the magnitude of the velocity component in the direction of PDV system sensitivity.

At the center of the PDV technique is the molecular filter, which provides the means for measuring the Doppler shift. The filter is a cylindrical glass tube filled with the vapor of a selected molecular species. The purpose of the filter is to convert frequency variations in the scattered light to intensity variations. The selected species, therefore, must have absorption lines near the frequency of the incident laser light. Doppler shifts arising from the flow velocity will then shift the scattered light relative to the absorption line, producing a variation in the transmission of light through the filter. Furthermore, by employing a pulsed laser, one can achieve time resolution equal to the pulse duration, for example, ~ 10 ns with a Q-switched Nd:YAG laser.

The roots of PDV can be found in the work of Shimizu et al.,[2] who proposed the combination of molecular filters and lasers to create a high spectral resolution light detection and ranging (LIDAR) system. Two groups of researchers introduced molecular filters to velocity measurements in the aerodynamic context. Miles et al.[3] showed that such filters could be used in wind-tunnel applications to suppress the scattering from walls and windows that can obscure the flowfield scattering. They also demonstrated that the time-averaged velocity at each pixel in a digital image of the flow could be obtained by acquiring images while scanning the laser frequency. Working independently, Komine and Brosnan[4] and Meyers and Komine[5] introduced the PDV technique (referring to it as Doppler global velocimetry) and pioneered several of the features common to many PDV systems. This approach relies on scattering from a particle-seeded flow, eliminating the need to scan the laser wavelength. Also, two flowfield images, viewing the flow with and without a filter, are acquired simultaneously and then ratioed to yield the scattering transmission. These works outlined many of the fundamental attributes of PDV and stand as the original proofs of concept.

Miles et al.[6] studied the characteristics of iodine molecular filters and described their use in conjunction with Nd:YAG lasers. Furthermore, their theoretical model of the iodine spectrum has

Received 4 February 1998; revision received 5 November 1999; accepted for publication 8 November 1999.

*Graduate Research Assistant, Department of Mechanical and Aerospace Engineering; currently Engineer, Adaptco, Melville, NY 11747.
†Assistant Professor, Department of Mechanical and Aerospace Engineering. Member AIAA.
‡Research Scientist, 2766 Indian Ripple Road. AIAA Associate Fellow.
§Aerospace Engineer, Air Vehicles Directorate; currently Air Force Office of Scientific Research Program Manager, Turbulence and Internal Flows, 801 Randolph Street, Arlington, VA 22203-1977. Member AIAA.

been widely used to calibrate the frequency axis of experimental iodine spectra.[7,8] Iodine filters have been studied by several other researchers with the goal of optimizing their performance.[9,10] Parameters considered have included the dimensions of the filter, the number density of the vapor as controlled by the temperature of the iodine reservoir, the use of a buffer gas to broaden spectral features, and the selection of the spectral feature to be used as the filter.

Predominantly, the continuous-wave single-mode, argon-ion laser ($\lambda = 514$ nm) and the injection-seeded, frequency-doubled, Q-switched Nd:YAG laser ($\lambda = 532$ nm) have been employed for PDV. The Q-switched Nd:YAG laser is an attractive choice because frequency tuning is easily accomplished through changing the voltage to the seed laser, the pulse durations are short (typically ~ 10 ns), and the pulse energy is large (up to ~ 1 J at 532 nm). Thus, even when the laser beam is formed into a large interrogating sheet, one can easily obtain strong scattering signals. However, several researchers have noted that the frequency of the injection-seeded Nd:YAG laser is subject to a long-term drift and a pulse-to-pulse variation, both of which can introduce errors into the velocity measurement.[7,8,10] Of course, one can simply monitor/record the mean drift over time,[11–13] but ideally the frequency should be recorded on a shot-to-shot basis.[10,14] This is most accurately and easily done by employing an additional iodine filter and sampling a portion of the interrogating laser beam.

The PDV technique has been assessed for accuracy in a number of ways. Several researchers have compared PDV measurements to known velocities on rotating wheels.[10,11,14] Clancy et al.[12] and Clancy and Samimy[15] developed two- and three-component PDV instruments, complete with a frequency-monitoring system, and compared PDV and LDV velocities recorded in a Mach 2 freejet. Here, the mean PDV velocities matched well the values from LDV, but there was some difference between the PDV- and LDV-derived turbulence intensities. A relatively recently recognized and significant source of error in instantaneous realizations of PDV is laser speckle. Smith and Northam[16] and Smith et al.[17] were among the first to call attention to the contribution made by this interference phenomenon to the noise that appears in single-shot PDV images. Here, the relative noise produced by speckle is proportional to the lens f-number and inversely proportional to the average dimension of the detector resolution element.[14,18]

Most PDV applications have been in relatively small facilities. Elliott et al.[9] used PDV to study compressible mixing layers. Smith and Northam[16] and Smith et al.[17] studied a sonic jet and an overexpanded supersonic jet, using spatial correlation techniques to show the organized motion of the shock diamond structure and interaction of the shock system with the large-scale structures in the shear layer. Smith[13] continued his study of supersonic jets by including a low-speed seeded coflow around the primary jet so that the full shear layer could be studied. Arnette et al.[19] developed a two-component PDV system and used it to study a compressible turbulent boundary layer; they were able to obtain mean velocity profiles that agreed with LDV measurements and provided superior near-wall resolution.

Meyers et al.,[20,21] Beutner et al.,[22] Meyers,[23] and Roehle[24] have focused on development of PDV for wind-tunnel applications. In the course of their work, which included experiments with delta wings and models of an F/A-18 aircraft, the high-speed civil transport, and a helicopter tail rotor, widely emulated data processing steps were introduced, including image mapping, pixel-sensitivity normalization, and low-pass filtering. In the work of Roehle,[24] the wake region behind an automobile was characterized with a PDV instrument that included a fixed camera view but multiple laser delivery angles, accomplished through fiber coupling the argon-ion laser output to the sheet-forming optics. Here, the planar velocity field (time averaged for 30 s) showed considerably greater spatial resolution than did LDV measurements made over a 2-h period.

Many of the PDV systems developed to date have recorded only a single velocity component. Early multicomponent PDV systems used two cameras per velocity component. Smith and Northam,[16] Smith et al.[17] and McKenzie[9] were among the first to combine side-by-side the filtered and unfiltered images on a single charge-coupled device (CCD) array. Other efforts to reduce the number cameras required include those of Arnette et al.,[19] who devised a scheme employing three cameras to measure two components, and Clancy et al.[12] and Clancy and Samimy,[15] who combined the pairs of filtered and unfiltered images on a single chip in measurements of multiple velocity components. Along these lines, Arnette et al.[25] have suggested a novel two-color method that combines signal and reference information onto a single-color CCD camera. In this scheme, two laser sheets having different frequencies are overlapped in the probe region. Scattering at the one laser frequency is absorbed by the filter (placed before the camera) according to the Doppler shift, while scattering at the other laser frequency is unaffected by the filter; the resulting composite image consists of alternating signal and reference pixels, obviating the need image mapping.

To end this review of the antecedents of the current PDV system that is based on interrogating a seeded flow, some examples of related techniques using unseeded flows are noted. Miles et al.[6] pointed out that time-averaged thermodynamic properties, pressure, density, and temperature, and velocity could be obtained from the gas-phase Rayleigh scattering by frequency tuning the laser across a filter transition. Shirley and Winter[26] and Elliott and Samimy[27] demonstrated a method capable of yielding instantaneous one-dimensional measurements of thermodynamic properties and velocity using an anamorphic lens for light collection. This lens images the scattered light at each viewing angle (up to ± 20 deg) along one dimension of the CCD. Consequently, the intensity at each viewing angle can be measured independently; in effect, one spatial dimension is sacrificed to obtain instantaneous quantities along the line of the laser beam.

Experimental Arrangements

Our PDV system, developed jointly at the Rutgers University Gas Dynamics and Laser Diagnostic Research Laboratory and at the U.S. Air Force Research Laboratory at Wright–Patterson Air Force Base, is shown in Fig. 1. The four chief components are the laser and sheet forming optics, the iodine filters, the laser-frequency-monitoring system, and the receiving optics and CCD cameras. Two similar frequency-doubled Nd:YAG lasers were used in the current experiments: a Spectra Physics GCR-170 providing 450 mJ per pulse with a Lightwave injection seeder (supersonic jet measurements), and a Spectra Physics GCR-150 providing 320 mJ per pulse with an Original Equipment Manufacturer (OEM) seeder (delta-wing measurements). Each laser performed similarly, operating at a repetition rate of 10 Hz with a pulse duration of ~ 10 ns. With injection seeding, the laser produces a narrow linewidth pulse (~ 100 MHz) whose center frequency can be tuned over a range of 70 GHz by applying a bias voltage to the seeder. The absorption line used in this study was at 18,789.28 cm^{-1}. A combination of spherical and cylindrical lenses formed the laser sheet that defined the measurement plane. For the jet experiments, the laser sheet was collimated; however, for the wind-tunnel experiments, this was impractical given the 30-cm-square probe region.

For PDV, the long-term frequency drift and pulse-to-pulse fluctuations necessitate a frequency-monitoring system. Measurements with our frequency-monitoring system (described subsequently) indicated that the standard deviation of the shot-to-shot laser frequency was 11 MHz in the small-scale laboratory (supersonic jet experiments) and 41 MHz in the large-scale wind tunnel. The higher level of fluctuation in the latter facility, in which the laser rested on top of the wind tunnel, was attributed to tunnel vibration. Without accounting for these frequency fluctuations, spurious velocity fluctuations would be measured in the flow: 4 m/s for the supersonic jet and 13 m/s for the wind tunnel. Clearly, this error is small relative to supersonic velocities but potentially large for subsonic values. Note also that several investigators have reported a chirp, or spatial variation in frequency, for the Nd:YAG laser of up to 150 MHz (Refs. 7, 8, and 15). The low level of the chirp in the current experiments, however, was confirmed in empty-tunnel tests where no spatial gradients in the frequency were observed.

Two iodine filters were used in the current system. Each filter cell is a glass cylinder, 7.6 cm in diameter and 25 cm in length, with flat windows at each end. A side arm and a small cold tip extend from the cylindrical body. Iodine crystals were placed in the side arm, and the cell was then evacuated. The cylindrical portion of the cell was wrapped with heating tape and insulation and was maintained at 378 K via a closed-loop temperature controller. The side arm was

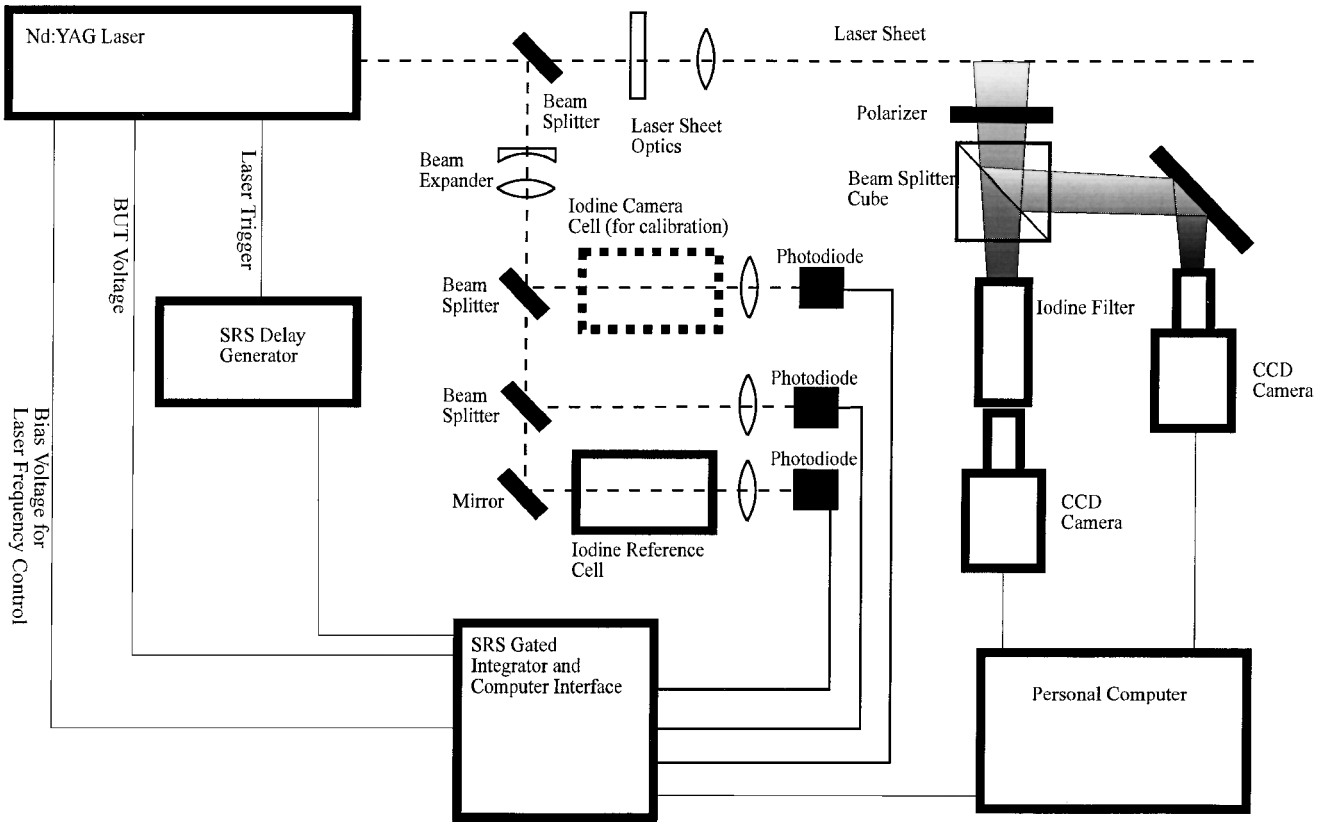

Fig. 1 Experimental arrangement for PDV.

maintained at a lower temperature, 313 K, by a constant-temperature water bath. After solid–vapor equilibrium was established in the side arm, a valve was closed shutting off the side arm from the cell body and fixing the number density of the iodine in the cell body. Such a filter is termed a starved cell because all of the iodine is in a gaseous state. In the current experiments, two cells with shut-off valves were not available, and consequently the constant-temperature water bath was used to control the iodine number density in the second cell. This type of cell is termed a saturated cell because vapor and solid exist in equilibrium. The starved-cell design results in a lower uncertainty because it is independent of the side-arm temperature once the valve is closed.[28]

Because one can easily add nitrogen to the cell (typically ~20 torr), the iodine transitions can be pressure (collisionally) broadened. The nitrogen was added after forcing essentially all of the iodine into the solid state by submerging the cold tip in a bath of dry ice and acetone. Once the desired pressure of the nitrogen had been set, the cold tip was reheated to the cell-body temperature. In the current experiments, both broadened (supersonic-jet experiments) and unbroadened (subsonic-delta-wing experiments) filters were used.

Figure 2 shows the effect of variations of three cell conditions: nitrogen partial pressure, side-arm temperature, and main-body temperature. These profiles have been normalized by the intensity measured with no iodine present in the cell; thus, they show the variation in the continuum absorption as well as the discrete absorption lines. Figure 2a shows the broadening effect as the partial pressure of the buffer gas is increased. Pressure broadening extends the range of measurable Doppler shifts for a given experimental geometry and, thus, is especially useful for supersonic flows. Figure 2b shows the effect of the side-arm temperature (or iodine number density) on the absorption profile with no nitrogen present. Increments of 5 K in side-arm temperature alter the cell performance dramatically. Therefore, in a saturated cell it is important to control the temperature of the coldest point in the cell precisely. Figure 2c shows clearly that the temperature of the cell body is not as important as the side-arm temperature inasmuch as the profiles overlie one another for a range of cell temperatures (373–413 K). The chief reason for keeping the cell at an elevated temperature is to prevent iodine condensation anywhere other than in the side arm.

A laser-frequency-monitoring system was implemented to compensate for the laser's pulse-to-pulse and long-term frequency variation and to characterize each filter's frequency-transmission relationship. The laser frequency associated with each PDV image was recorded through the use of a second iodine filter, termed the frequency-monitoring filter. As seen in Fig. 1, a portion of the laser beam was directed to the frequency-monitoring/calibration system. This beam was first expanded (to a 25 mm diameter, to prevent saturation of the iodine transitions) and was subsequently divided into three parts, using Inconel-coated beam splitters. Two of the beams were directed through the frequency-monitoring and camera filters, when calibrating the iodine filters, and then onto high-speed photodiodes (Thor Laboratories DET210); the remaining beam was sampled by a reference photodiode (without passing through a filter) and accounted for shot-to-shot beam energy fluctuations. The filter transmission is then simply given by $S_{\text{filter}} / S_{\text{reference}}$. In each case, the beam was focused onto a flash-opal diffuser located about 25 mm in front of the respective photodiode; this ensured that the photodiode signal was insensitive to alignment variations. Each photodiode signal was detected by a Stanford Research Systems gated integrator (SR250). Typically, the sampling gate for each SR250 was set to about 50 ns; triggering of the gated integrators was accomplished using either the Q-switch signal from the laser or the Transistor Transistor Logic (TTL) pulse from a Stanford Research Systems delay generator (DG535). The SR250 output voltage was digitized to 12-bit accuracy with the Stanford Research Systems computer interface (SR245). The SR245 was interfaced to the personal computer and the custom software through an Institute of Electrical and Electronics Engineers 488 port.

Other SR245 ports were employed to control the laser-frequency set point and to record the voltage associated with the Q-switch buildup time. This voltage indicates whether the laser pulse is composed of a single longitudinal mode. For buildup-time voltages greater than a given value (specific to each laser), the laser pulse is composed of multiple longitudinal modes; an image associated with a multimode pulse was, of course, discarded. This was an important feature for successful wind-tunnel measurements because vibrations caused the laser to operate multimode for some of the laser pulses. To demonstrate the efficacy of this approach and the

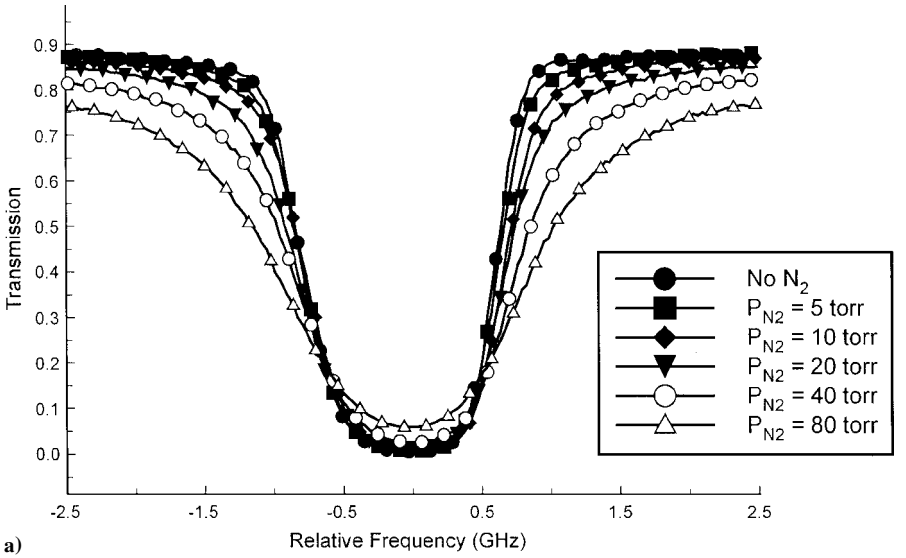

a)

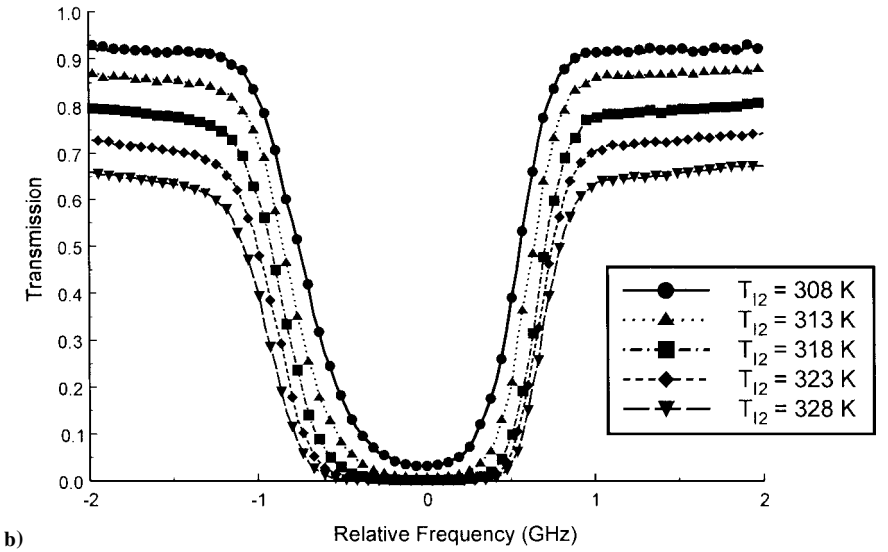

b)

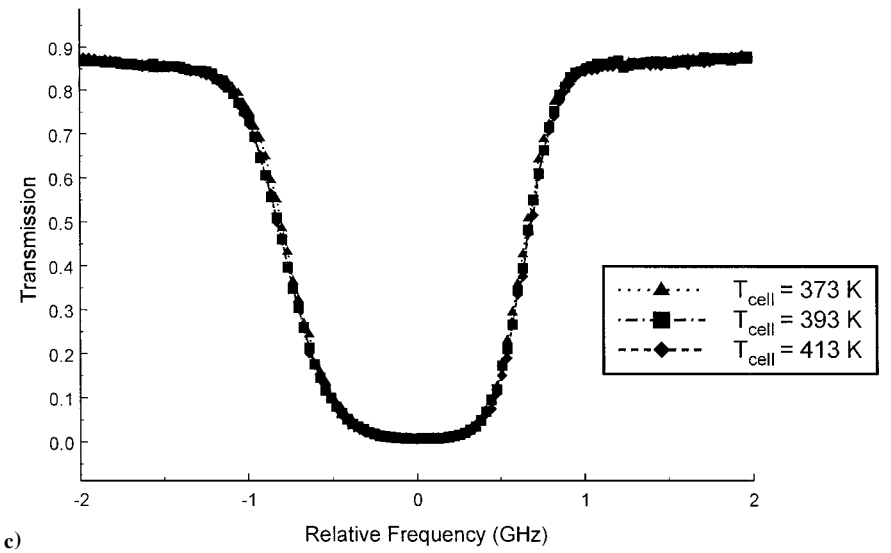

c)

Fig. 2 Effects of cell conditions on filter performance. For the nominal side-arm temperature (T_{I2} = 313 K), iodine partial pressure was estimated to be 1.0 torr and nominal conditions are a 373-K body temperature, a 313-K side-arm temperature, and no buffer gas. Varied conditions are a) nitrogen, buffer gas, partial pressure; b) side-arm temperature; and c) filter-body temperature.

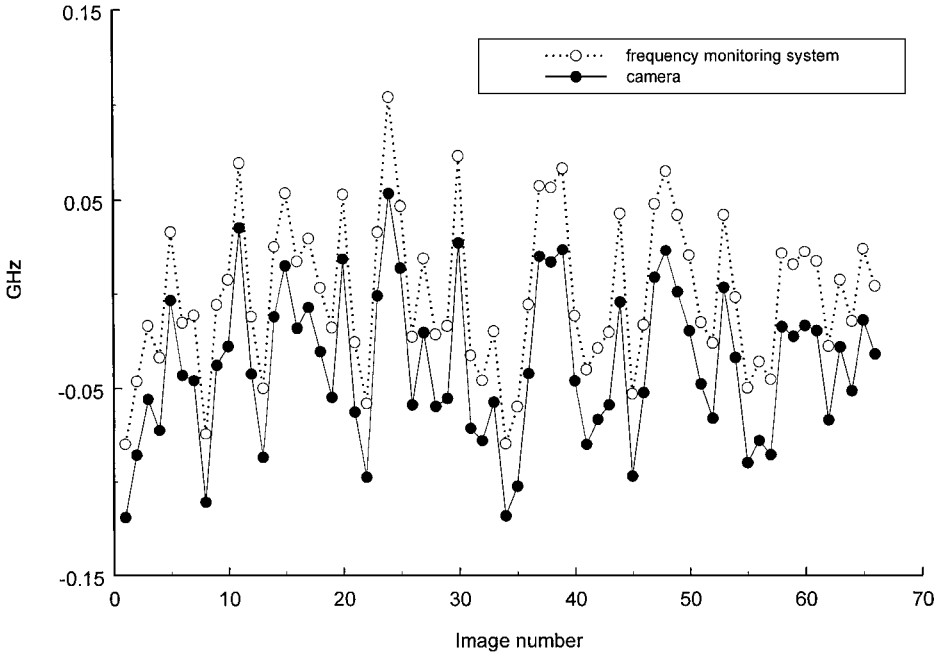

Fig. 3 Frequency for 66 laser pulses as measured by the frequency-monitoring system and by the PDV camera system in a uniform Mach-0.2 flow; difference between the two frequency measurements has an rms of less than 4 MHz.

frequency-monitoring system in general, we recorded laser frequencies in the empty-tunnel flow. In Fig. 3 we show the frequency derived from the monitoring system and from the PDV cameras. To minimize the effects of turbulence and speckle on the frequency inferred from the camera measurements, and therefore focus on the performance of the wavelength reference system, we averaged the signal from a group of pixels. The rms of the laser frequency, from either the cameras or frequency-monitoring system, was 41 MHz, but the rms of the difference between the frequency-monitoring and the camera measurements was less than 4 MHz. This demonstrates that the precision of the frequency-monitoring system is better than 4 MHz; in fact, this number includes noise contributions from the camera frequency measurement and the flow (through velocity variations).

The receiving optics consisted of a polarizer followed by a 7.6×7.6 cm cube beam splitter providing separate optical paths to two 16-bit back-illuminated PixelVision CCD cameras (Model SV512V1), each having a 512×512 array (with 24-μm-square pixels). These cameras were fitted with Nikon 105-mm micro-Nikkor lenses, set to an f-stop of 5.6. The purpose of the polarizer was to reduce polarization-dependent scattering variations that might occur in the flowfield and through the optical system. Also, the polarizer was expected to reduce the background intensity relative to the particle-scattering intensity. The purpose of the beam splitter was to ensure that the viewing angles of the signal and reference cameras were identical. The signal camera viewed the flow through a molecular iodine filter, while the reference camera viewed the flow without a filter. Camera exposure times were set to 60 ms using the integrated mechanical shutter. The measurement timescale, however, was determined by the 10-ns duration of the laser pulse rather than by the camera exposure time.

As already noted, some investigators have combined both signal and reference images onto a single CCD chip. Although this approach reduces the number of cameras required, especially valuable when measuring multiple velocity components, it has two disadvantages: 1) The number of available pixels is reduced by a factor of two. 2) The signal and reference images may overlap to some degree, as discussed by McKenzie.[10] The extent of the overlap is dependent on the aperture setting of the lens that follows the image-splitting apparatus. Though small apertures decrease the overlap, there is an imperative in instantaneous PDV measurements to open the aperture to minimize laser speckle.[14,18] Also, by properly masking the overlapping region near the object plane, or by having a dark field adjacent to the measurement region, this effect can be reduced.

Axisymmetric Jet Facility

To demonstrate its capabilities, our PDV system was tested on a small-scale supersonic jet. This flowfield was selected because it was expected to offer a minimum of complications. It could be well seeded (at least in the core) so that large scattering signal levels could be achieved. Furthermore, it provided easy optical access with very little secondary scattering from the flow facilities. The apparatus itself was relatively small, and the PDV system and laser could be isolated from the flow facility so that the effect of vibration was negligible.

The jet experiments were performed at the U.S. Air Force Research Laboratory, Wright–Patterson Air Force Base. The jet issued vertically through a Mach 1.36 converging–diverging nozzle designed by the method of characteristics (12.7-mm exit diameter). The stagnation pressure was 283 kPa, and the stagnation temperature was $\sim$294 K. The flow was seeded with ethanol, which was injected into the stagnation chamber. It was estimated that the particle size of the condensed ethanol was on the order of 30 nm (Refs. 3 and 19). The laser sheet contained the axis of the jet, with the direction of laser propagation making an angle of 10.1 deg with respect to the jet axis. The viewing direction was normal to the laser sheet so that the measured velocity component was at an angle of 45.8 deg relative to the jet axis.

For comparison with PDV, the velocity of the jet was measured with a two-component coincident LDV system. A TSI color-burst system was used to compute the Doppler shifts. From these two-component LDV measurements, it was possible to find the mean velocity component in the direction measured by the PDV system. LDV-derived velocities were recorded at several axial locations, including two that corresponded to regions in the PDV imaged area at values of $x/D = 3$ and 7. For the LDV measurements, the flow was seeded with 0.5-μm aluminum–oxide particles.

Subsonic Wind-Tunnel Facility

The delta-wing experiments were performed at the U.S. Air Force Research Laboratory's Subsonic Aerodynamic Research Laboratory wind tunnel (Air Vehicles Directorate, Wright–Patterson Air Force Base). Much of the interest in PDV is rooted in its presumed ability to provide high-spatial-resolution measurements in large facilities. A principal purpose of the wind-tunnel tests was to demonstrate this. The delta-wing flowfield was selected because of the interest in the interaction of leading-edge vortices with tails and because the test flowfield had been simulated with a computational fluid dynamic (CFD) model.[29]

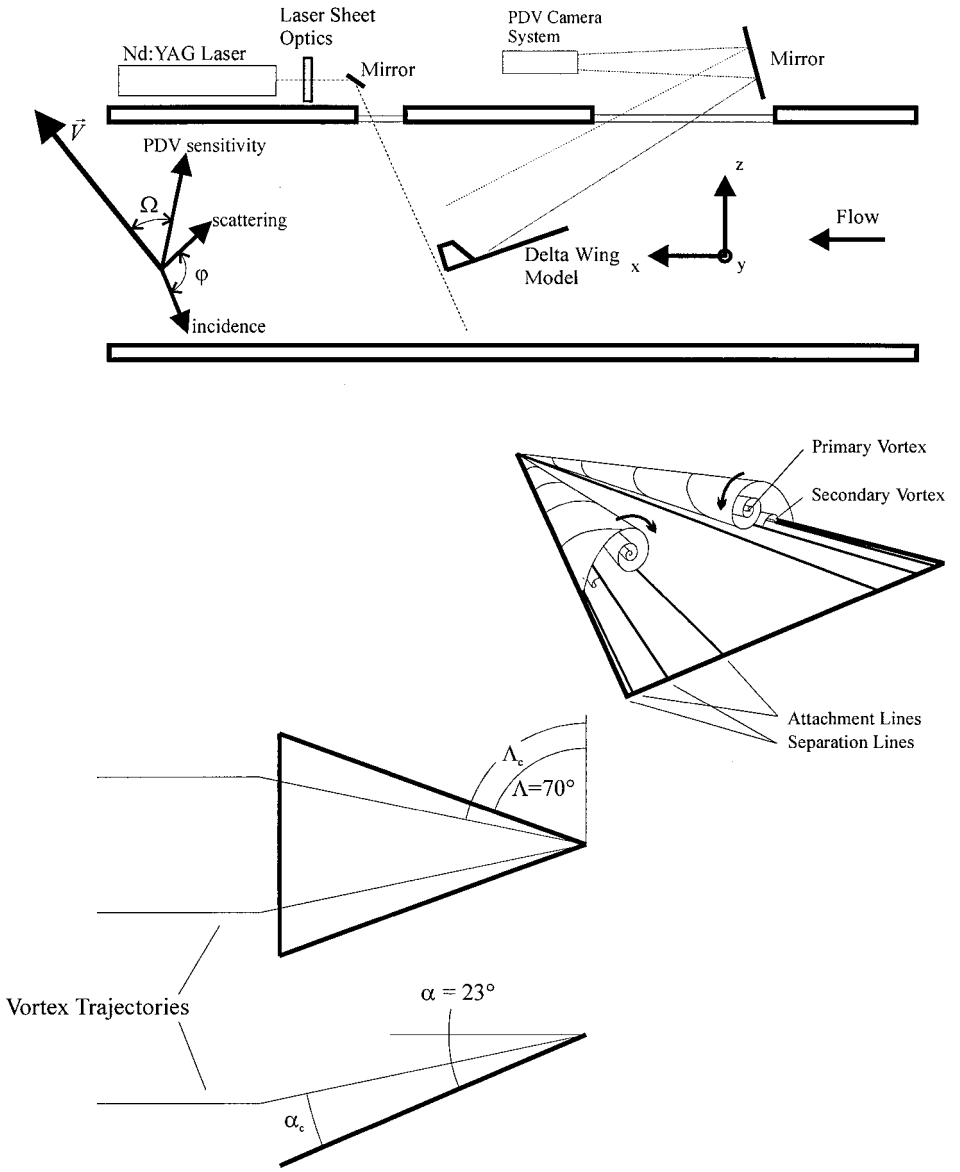

Fig. 4 Geometry of PDV measurements in the Subsonic Aerodynamic Research Laboratory and schematic of the flow over a delta wing.

In applying PDV in large-scale facilities, several difficulties not present in the smaller-scale laboratory must be addressed. The test environment is relatively harsh, with larger extremes of temperature, vibration, and acoustic noise. The temperature variations necessitate that the iodine-cell conditions are well controlled and that the laser frequency drift is monitored and recorded. The vibrations can cause the laser to fluctuate in frequency much more than normal (as already noted) and in general will require vibration isolation so that the laser remains seeded. Even the sound generated by the wind tunnel was found to degrade laser-seeding performance. To be successful in a large wind-tunnel environment, effects of vibration must be mitigated: For example, rigid optical mounts should be used and camera lenses must be secured so that they will not vibrate out of focus. Because the system is more sensitive to day-to-day changes in the unregulated environment of the large-scale facility, iodine-filter absorption profiles and camera-calibration images were taken at the beginning and end of each day. This required that the alignment and placement of dot- and calibration-cards be repeatable and easy. An additional problem encountered in large-scale facilities is more limited optical access. As a result, the laser sheet may be viewed at oblique angles, limiting the lowest f-stop that can be used without excessive image blur. Optical access limitations also result in PDV system sensitivity directions that are generally not aligned with the desired velocity components (at least to the degree possible in smaller facilities). A final complication is that the data should be analyzed quickly so that errors are quickly detected and tunnel time is not wasted on data that would later be discarded.

Figure 4 shows the PDV arrangement with the delta wing in the test section of this facility. It is an open-circuit, low-speed wind tunnel with a 3.05 ×2.13 m test section. In the inlet, a movable multiport, smoke-generating rig was available to seed the flow. This seeding apparatus permitted the seeding of a stream tube in the flow having an area on the order of 1000 cm^2. Based on comparable seeding systems, the seed particles were expected to have diameters characterized by a log-normal probability distribution with a most likely diameter on the order of 1 μm (Refs. 10 and 20). The model was a 70-deg-sweep delta wing with sharp leading edges, set at an angle of attack of 23 deg. Measurements were obtained on the wing at four different chord locations (85.7, 97.1, 102.9, and 114.3% chord) at a freestream Mach number of 0.2. This corresponded to a freestream velocity of 68 m/s and a root-chord-based Reynolds number of 1.87×10^6. At this condition, no vortex bursting was present over the model surface. Measurements were also made of the same model equipped with two vertical tails. These tails had a 35-deg leading-edge sweep and unswept trailing edges. Their trailing edges were aligned with the trailing edge of the wing, and their position was chosen to lie along rays emanating from the apex at 64.3% span. This position was chosen to approximate the vortex-core trajectory for the clean delta wing. The measurements were made at the same chord locations, angle of attack, and freestream velocity as the measurements for the clean wing.

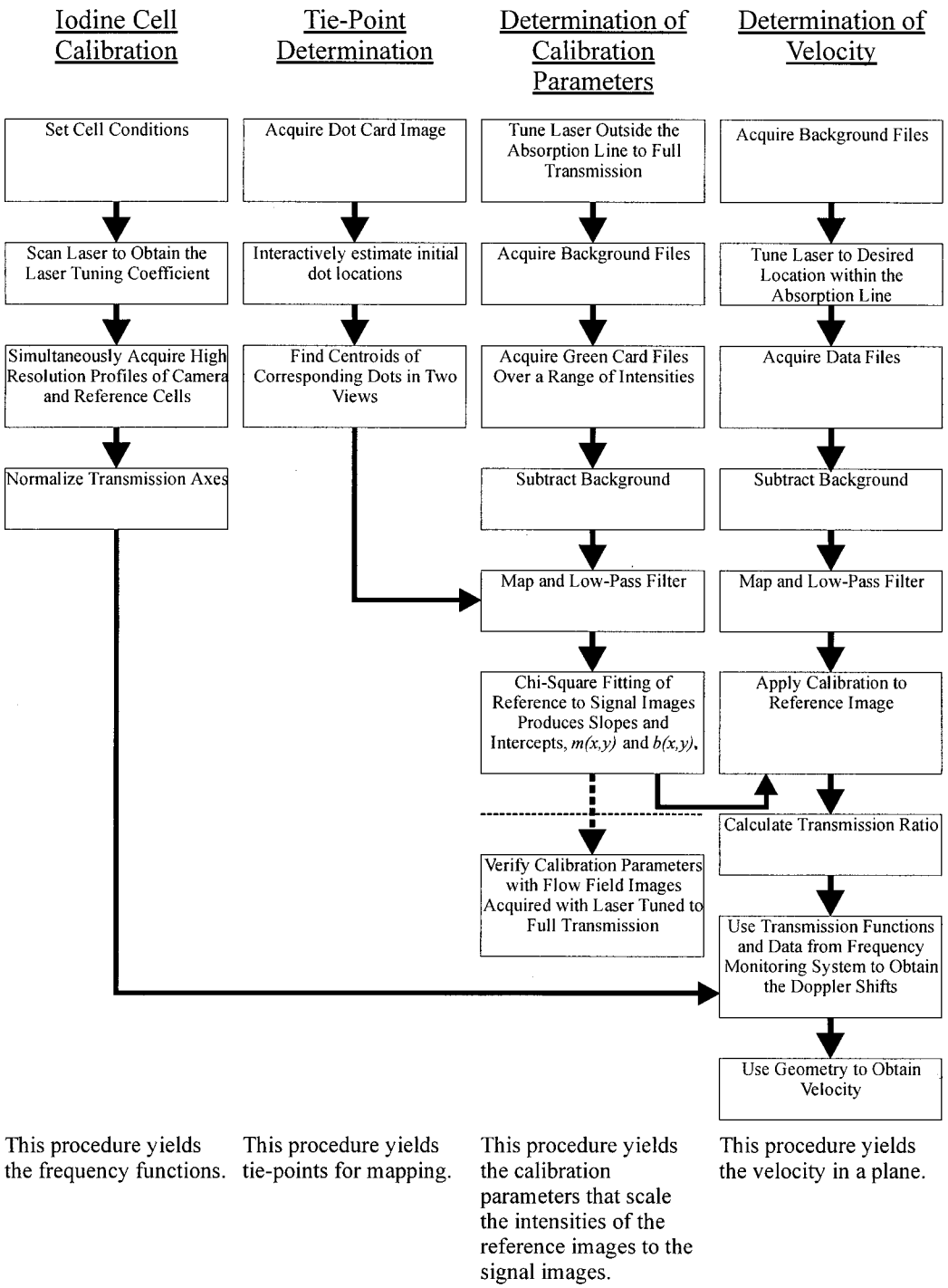

Fig. 5 Procedure for PDV measurements.

The laser sheet was oriented spanwise across the tunnel with a propagation direction normal to the model surface (Fig. 4). The direction of PDV sensitivity, based on this geometry, was $-0.210\boldsymbol{i} - 0.003\boldsymbol{j} + 0.978\boldsymbol{k}$. The velocity component measured was, thus, predominantly vertical and slightly upstream. This direction was chosen because its velocity component was strongly affected by the leading-edge vortices and was the simplest to implement in the tunnel with the current optical access. Because measurements were sought between the tails, it was necessary to impinge the model with the laser sheet. Of course, this is not ideal because the surface scattering is much stronger than the particle scattering in the vicinity of the impingement.

Data Processing

The following four steps are required in the current implementation of PDV: 1) Calibrate the iodine cells to determine the transmission-frequency relationships. 2) Find the tie points to overlap views of the two cameras. 3) Determine the calibration parameters, that is, those that scale the intensity of the reference images relative to that of the signal images. 4) Calculate the velocity using the data images and the information obtained in steps 1–3. This procedure is shown schematically in Fig. 5 and described in detail next.

Iodine Cell Calibration

The conditions for the two cells (side-arm temperature, body temperature, and partial pressure of buffer gas) were set according to the expected velocity ranges. Before flowfield measurements were made, the camera filter was moved to its calibration location (Fig. 1). Both cells were then calibrated simultaneously. Calibration consisted of scanning the laser frequency (by incrementing the voltage from the SR245 output port) while measuring the transmission of the iodine cells.

Table 1 PDV system characteristics for jet and wind-tunnel experiments

PDV characteristic	Jet facility	Wind-tunnel facility
ϕ	90 deg	110.8 deg
Ω	45.8 deg	102.1 deg
$(\partial V/\partial\phi)/V$	−0.9%/deg	−0.6%/deg
$(\partial V/\partial\Omega)/V$	1.79%/deg	−8.16%/deg
Sensitivity, $(2/\lambda)\sin(\phi/2)$	2.66 MHz · (m/s)	3.10 MHz · (m/s)
Sensitivity^{-1}, $[(2/\lambda)\sin(\phi/2)]^{-1}$	0.376 (m/s) · MHz	0.323 (m/s) · MHz
Spatial resolution	0.16 mm/pixel	0.98 mm/pixel
$d\zeta_c/d$ (% transmission)	−6.1 MHz/(% transmission)	4.4 MHz/(% transmission)
$d\zeta_r/d$ (% transmission)	−7.6 MHz/(% transmission)	4.1 MHz/(% transmission)

The raw data from the calibration consisted of ordered pairs of data for the camera filter and for the frequency-monitorfilter. In each case, the abscissa was the voltage to the seed laser and the ordinate was the ratio of the gated-integrator voltage from the filtered photodiode to that from the unfiltered (reference) photodiode. Before these ordered pairs of data could be used, the abscissa needed to be converted from units of seeder voltage to units of frequency. This conversion was performed by identifying features of the iodine spectrum (from the calibration scan) and comparing their separation in terms of voltage to their known separation in terms of frequency.[7,8] For the velocity measurements, only the approximately linear portion along one side of a single absorption line was used for frequency discrimination. The low-frequency (red) side of the line, which possesses a shallower slope than the high-frequency (blue) side, was used in the jet experiments, whereas the blue side was used in the wind-tunnel experiments. These choices were made to increase the respective range and sensitivity for jet and wind-tunnel experiments.

The method just outlined resulted in transmission curves for the two filters, the camera filter and the frequency-monitorfilter, having a common abscissa (relative frequency); however, the ordinates of these curves were independent of one another. Differences in the performance of the beam splitters, the optical paths, and the gated integrators meant that the voltage ratios representing the transmission of the filters had undetermined scales. Each curve was normalized by its maximum transmission within the range used for frequency discrimination, resulting in normalized transmission that varied from ~0 to 1. Inverting the axes of these curves produced functions of frequency vs transmission for the camera filter, ζ_c, and for the frequency-monitor filter, ζ_r. The former function is used to establish the shifted frequency of the light scattered into the PDV optical system at each pixel, and the latter function is used to establish the frequency of the laser pulse. Table 1 gives approximate values for their slopes in the linear region.

Tie-Point Determination

It was necessary to align the fields of view for the two cameras so that they overlapped as nearly as possible before taking their ratio on a pixel-by-pixel basis. To accomplish this alignment, the following steps were taken.

A card that filled the fields of view of both the signal and reference cameras was placed in the image plane (plane of the laser sheet). This card was marked with a rectilinear pattern of dots. The centers of these dots were found to subpixel accuracy (0.1 pixels) by finding the intensity-weighted centroid in the region surrounding each dot. In later stages of the data reduction, the output of the dot-finding program was used to map pairs of signal- and reference-camera images so that they corresponded on a pixel-to-pixel basis. The mapping program used bilinear interpolation to locate a source pixel in the unmapped image for every pixel in the mapped image. The location in the source image was not generally given by integer pixel values. Therefore, the intensity value assigned to the mapped image was calculated as a weighted average of the nearest four pixels.

After the mapping, the images were low-pass filtered, to reduce the speckle noise, by replacing the value at each pixel with the average of the 25 pixels (5 × 5 matrix) in the region centered at that pixel. This level of filtering was selected to give low random error while maintaining a spatial resolution sufficient to capture the flow features of interest. For the jet measurements, the size of individual pixels mapped into the object plane was 0.16 mm; for the subsonic wind-tunnels measurements, this value was 0.98 mm. Clearly, however, we have lowered the spatial resolution (by smoothing) in an effort to reduce noise in the velocity images; if one can tolerate increased noise in the velocity image, fewer pixels are needed for the low-pass filter. Because the noise-to-signal ratio (NSR) is inversely proportional to the average number of speckle cells within each resolution element,[14,18] we effectively increase the number of speckle cells, and decrease the NSR, within each resolution element by binning. Furthermore, apart from effects such as image blur and mapping errors (which create a correlation in signal from one pixel to the next), we expect that the speckle noise will, thus, decrease proportionally with $1/N_b$, where N_b is the binning number, for example, $N_b = 5$ with 5 × 5 binning. As noted earlier, one can lower the speckle noise without also degrading the spatial resolution by increasing the lens aperture.[14,18] In the jet experiments, for example, the NSR of the recorded scattering (without low-pass filtering) was reduced from about 7.6 to 4.2% when the lens f-stop was decreased from 5.6 to 2.8. However, in practice image blur, which will be more likely with oblique views in large-scale facilities, may limit the optimum aperture setting.

Calibration for Electronic Gain and Optical Path Differences

In addition to the described mapping procedure, a calibration procedure was necessary so that the ratios recorded by the camera systems corresponded to the camera frequency function ζ_c, which had been established with the frequency-monitoring/calibration system. To determine the calibration parameters, a series of images, termed the green-card images, was acquired at the frequency of maximum transmission. These images were used to scale the reference-image intensities to those of the signal images. The calibration method for the tunnel experiments is described next.

A uniform card was placed in the image plane. The laser beam was diverted and directed through a diffuser such that it illuminated the green card. Several background images were acquired with the laser on but blocked. These images were subtracted from subsequent green-card images so that the bias of stray background light was removed. In the subsequent images, neutral density filters were placed in the path of the laser beam. The result was a wide range of illumination intensities for the series of green-card images.

After the background subtraction step, the images were mapped and low-pass filtered. Because these images were acquired at the maximum transmission, the ratio of the signal to reference images should be unity on the normalized scale of the camera frequency function ζ_c. Therefore, calibration parameters, slope and intercept determined from a least-squares fit, were found to match the signal and the reference images at each pixel. Because of the background subtraction, the values of the intercept were expected to be close to zero, and this was indeed the case. Conducting a least-squares fit enables the linearity of the camera to be verified; though this not an issue for most CCD detectors, we have noted some nonlinearity in the response of intensified CCD cameras.

Determination of Velocity

The preceding outlined steps provided all of the necessary mapping and calibration data. The series of steps in the fourth column of Fig. 5 were then necessary for PDV measurements. Background

images were acquired with the laser on and tuned to maximum transmission, but with the flow seeding off. These images were subtracted from subsequent particle-scattering images so that the bias of stray background light was removed.

A series of data images was then acquired. The laser was tuned to the position deemed appropriate for the flow under investigation. For the vortical flow above a delta wing, this position was near the middle of the blue side of the transition because both positive and negative Doppler shifts were expected. For the jet, on the other hand, this position was near the shoulder of the red side of the transition because all of the Doppler shifts were expected to be positive and some were expected to be so large as to require nearly the full linear portion of the absorption line.

After subtraction of the background, the signal and reference images were then mapped and low-pass filtered. The reference images were then modified using the previously determined slopes and intercepts. The signal images were then divided by the calibrated reference images, producing a series of images containing the transmission at each pixel. The transmission was then converted to relative frequency using the function ζ_c. Similarly, the transmission measured by the frequency-monitoring system was converted to frequency with the function ζ_r.

The difference between the relative frequency at a given pixel and the relative frequency of the laser for that particular image is the Doppler shift for that pixel. This Doppler shift may then be converted to velocity through the Doppler-shift equation:

$$V\cos(\Omega) = [\lambda/2\sin(\phi/2)][\zeta_c - \zeta_r] \tag{2}$$

where the term in brackets is the Doppler shift expressed in terms of the frequency functions.

Table 1 lists some of the important parameters for the PDV system as it was arranged for the jet and wind-tunnel experiments. The angle ϕ between the laser propagation direction and the scattering direction is a right angle in the jet experiments and just slightly obtuse in the wind-tunnel experiments, affording relatively flat views

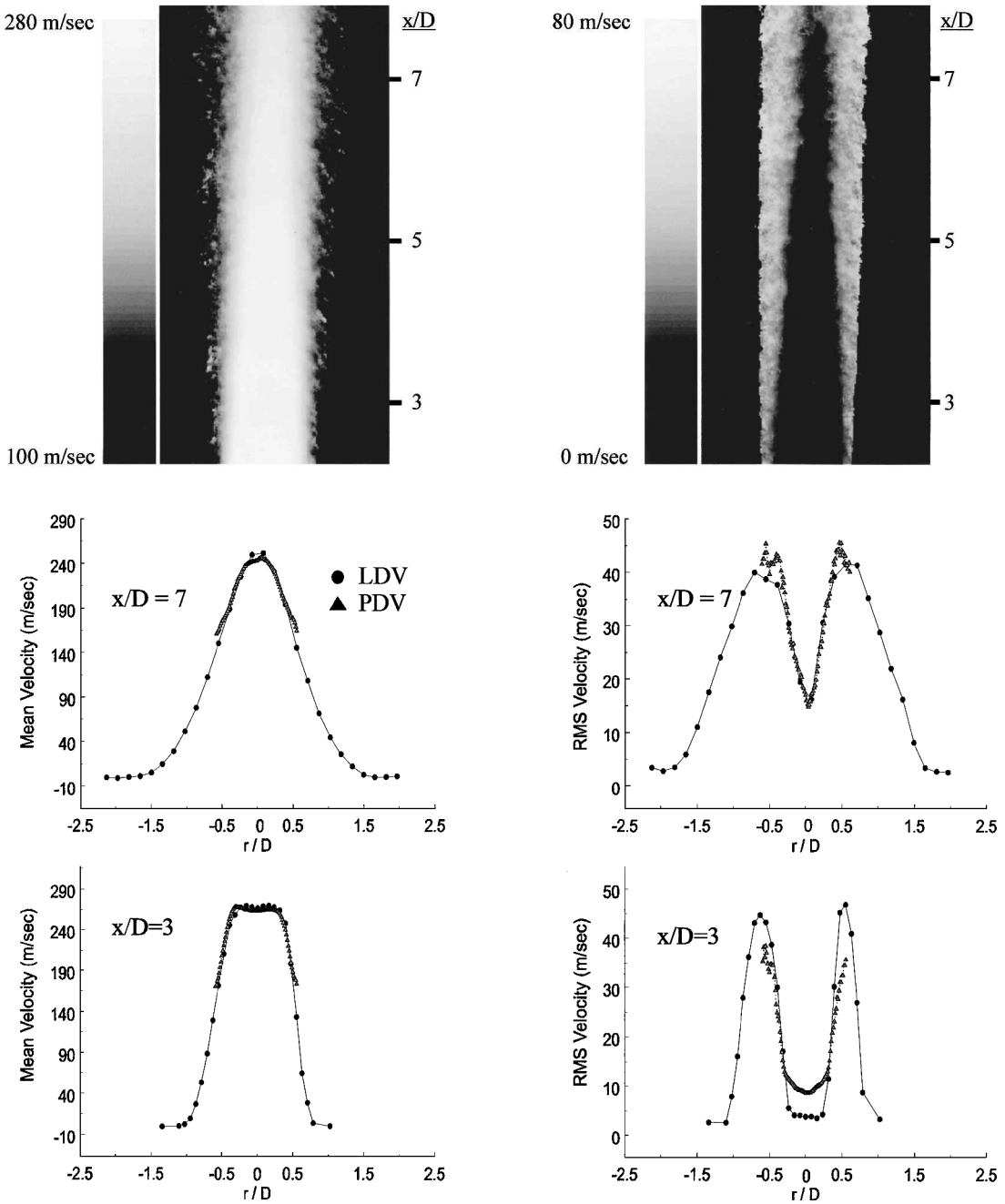

a) Comparison of averaged PDV and LDV measurements **b) Comparison of the rms of velocity fluctuations**

Fig. 6 Mach-1.36 jet: circles represent velocities from LDV, and triangles show values from PDV.

of the laser sheet. The angle Ω specified in Table 1 assumes that the velocity vector in the jet case is directed entirely along the jet axis, a good assumption for the mean flow in the center of the jet. For the wind tunnel, Ω is specified only for the empty-tunnel measurements for which the assumed direction of the velocity vector is in the downstream tunnel direction. The next two listings in Table 1 are the relative errors in velocity per degree of error in the angular measurements. Though the velocity measurements are relatively insensitive to small errors in Ω, in the wind tunnel Ω is not well chosen to measure the freestream velocity. A different PDV geometry would have been selected if that had been the goal of these experiments. The sensitivity and inverse sensitivities, also given in Table 1, provide convenient means for converting PDV system measurements between units of velocity and frequency. The slopes of the frequency functions give an indication of one of the compromises in PDV. The smaller the magnitude of the slopes, the less sensitive the system is to errors in measuring the transmission. However, small slopes also imply a lower limit on the frequency (or velocity) range measurable by the system. Thus, the wind-tunnel arrangement is less sensitive to transmission errors, but its range is only on the order of 440 MHz (140 m/s) compared to 610 MHz (230 m/s) for the jet arrangement. It should be emphasized that in this procedure for measuring velocity using PDV, there is no need to calibrate the system using a known velocity in the flowfield; that is, flows where the velocity is unknown can easily be investigated.

Results

Results are first presented for the Mach 1.36 jet. In Fig. 6, flow is from bottom to top with the imaged region of the jet extending from x/D equal to 2.22–7.91. The left-hand column shows the average velocity field based on 100 instantaneous images. Also shown are plots of the PDV- and LDV-derived velocity profiles at two axial stations ($x/D = 3$ and 7). Here, PDV and LDV yielded approximately the same mean values. In addition, three downstream locations were analyzed in detail: The difference in the average LDV- and PDV-derived velocities was between 4 and 8 m/s out of ~260 m/s (the PDV velocities were consistently below those from LDV). Both techniques yield mean core measurements that are below the value obtained from isentropic theory for the Mach 1.36 jet, $V_{isen} = 278$ m/s, probably indicating that the Mach number was actually less than the design value of 1.36.

Both measurement techniques show the thickening of the shear layer with downstream position; however, acceptable PDV data did not extend far into the shear layer. Presumably, the primary reason is that the volatility of the PDV seed medium, ethanol, results in diminished seeding in the warmer shear layer; this is particularly

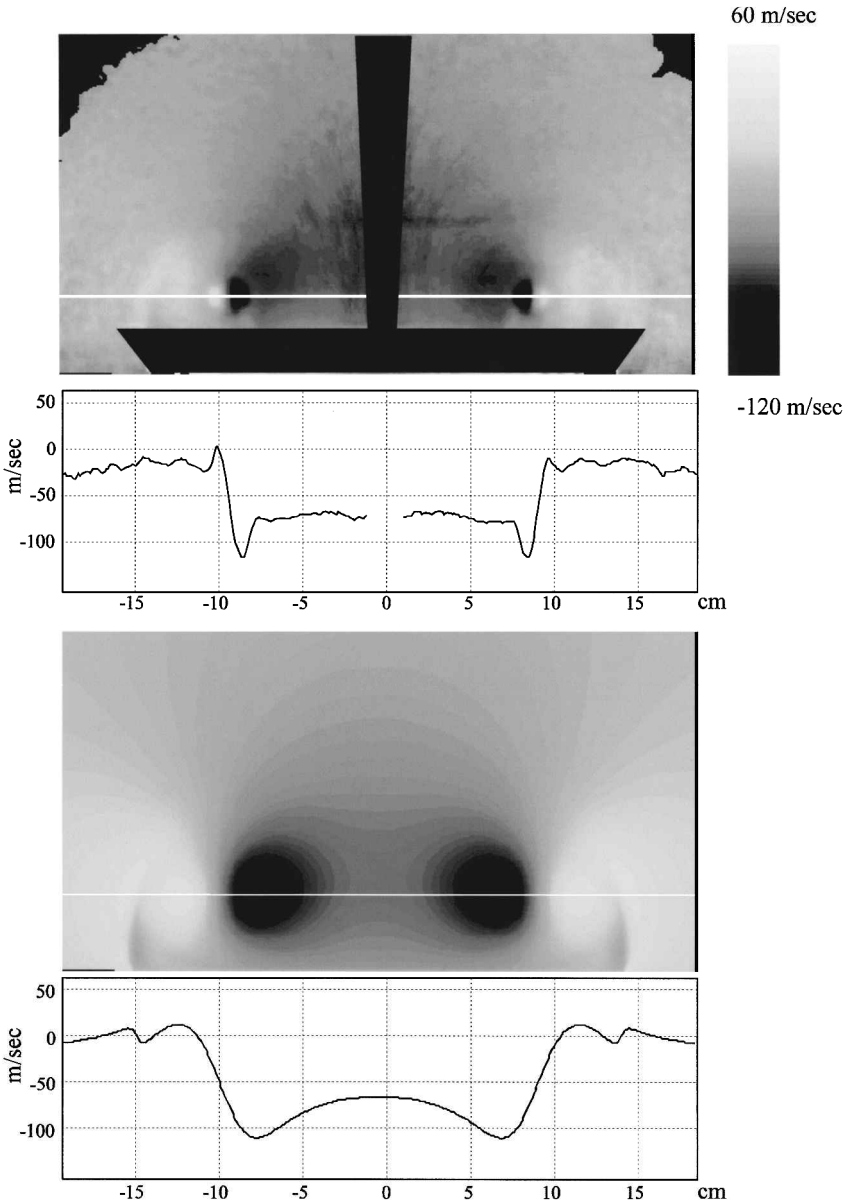

Fig. 7 Average PDV measurements of the flow over a delta wing at 86% root chord with comparison to the CFD simulation.[29]

problematic for modest Mach supersonic numbers, for example, 1.36. Furthermore, the intermittency of the shear layer means that even with adequate seeding, a sample of 100 images might not yield sufficient data for accurate mean readings throughout the shear layer. This deficiency is not a limitation of the PDV system, but more a characteristic of the seeding available at the time of the test. Of course, the LDV technique was more successful at measuring into the shear layer because more samples were acquired and the seed did not evaporate in the shear layer. Nonetheless, with thermodynamically insensitive seeding, PDV can also resolve jet velocities throughout the shear layer.[13,14]

The right-hand side of Figure 6 gives the rms of the PDV velocities along with plots of the rms velocity obtained by PDV and LDV at $x/D = 3$ and 7. The image and the line plots show the expected trend of low turbulence levels in the core with increasing turbulence levels in the jet periphery. Again, fewer points were used to calculate the rms of the PDV velocities in the shear layer than in the core because of the intermittent nature of the shear layer. From the LDV measurements, it can be seen that the centerline turbulence increases with downstream distance. The PDV results agree well with the LDV results at the $x/D = 7$ station. Upstream of this, LDV-derived velocity fluctuations fall to about 4 m/s. The PDV measurements follow the LDV results fairly well off the centerline but reach a minimum of ~9 m/s; this minimum is believed to represent a combination of the noise of the measurement technique (resulting primarily from speckle) and the true fluctuation in the flow added in quadrature.

Prior to measuring the complicated flow above a delta wing, measurements were made in the wind tunnel without a model in place at Mach numbers of 0.2 and 0.3 (corresponding to respective freestream velocities of 68 and 96 m/s). Here, the purpose was simply to gain insight into the system performance within the wind tunnel. The expected velocity components in the direction of PDV sensitivity and the measured velocity components differed by 1.7 m/s (5.3 MHz) and 0.5 m/s (1.6 MHz) for the Mach 0.2 and Mach 0.3 conditions, respectively; the corresponding random errors were 3.8 and 3 m/s. Surprisingly, these errors are much smaller than the ~100-MHz laser linewidth. In relative terms, these bias errors, 12 and 2.5% of the respective component velocities of 14 and 20 m/s, may seem unacceptably large; however, it should be emphasized that the PDV system was not optimized for streamwise velocity measurements. It is expected that these errors, ~1 m/s, represent the system detection limit. Note that an analysis by Beutner et al.[30] using the same data set, but with independent data processing routines, yielded similar results.

Before presenting the measurement results for the delta wing, a basic description of the flowfield will be provided following

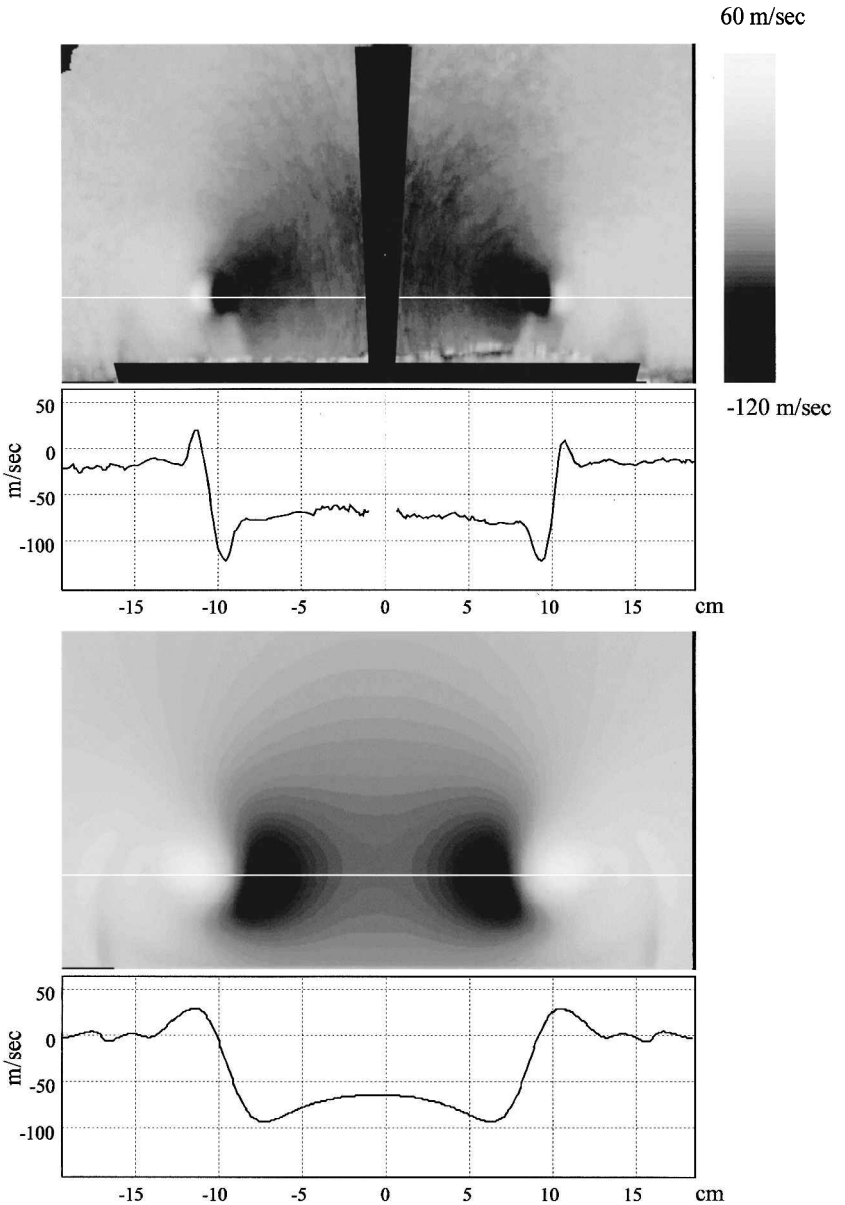

Fig. 8 Average PDV measurements of the flow over a delta wing at 97% root chord with comparison to the CFD simulation.[29]

Visbal.[31] A highly swept wing at an angle of attack α experiences boundary-layer separation at its sharp leading edge. The three-dimensional shear layer that rises over the wing then spirals into a pair of counter-rotating vortices (Fig. 4). The vortices follow approximately straight-line trajectories over the wing and are characterized by a vortex sweep angle Λ_c and an inclination angle α_c relative to the wing surface. In the near-wake region, the vortices become aligned with the freestream flow.

In the core of the vortices, the azimuthal velocity component is proportional to radial location, which is the defining characteristic of solid-body rotation. The vortex cores also show strong jetlike behavior with the maximum axial velocity within the core achieving values up to twice the freestream velocity. The circulation exhibited by the cores increases with axial distance as vorticity from the feeding sheet is entrained into the vortex. An important phenomenon associated with delta-wing flows is vortex bursting. With an increase in angle of attack, flow instabilities can arise that cause a region of reversed flow along the vortex axis accompanied by dramatic growth of the vortex core. This phenomenon may be transient, oscillatory, and asymmetric. Vortex bursting is of great interest because it can lead to sudden changes in aerodynamic forces and moments that can adversely effect the performance of delta-wing aircraft.

Figures 7–10 show frame-averaged PDV measurements at the noted locations based on 50, 50, 62, and 59 images, respectively. Each image shows the vortical structure that is characteristic of the flow over a delta-wing at an angle-of-attack. Recall that the PDV system was sensitive to a velocity component in the direction $-0.210\boldsymbol{i} - 0.003\boldsymbol{j} + 0.978\boldsymbol{k}$. The particularly strong negative velocities are indicative of the large streamwise velocity component in the vortex core (the jetlike behavior) coupled with a large downward component on the inboard side of the vortex. In the first three images, the delta wing is in the field of view. No reliable data can be extracted from these regions near the wing due to the strong surface scattering. Similarly, scattering from the sting supporting the wing corrupted the data in the center of the flowfield. Nevertheless, large areas of the imaged region were available for velocity measurements. A plot of the velocity along a line drawn through the cores is also given for each image. The nearly linear region in these profiles is indicative of the vortex cores. The vortex angle of inclination, α_c, was found to be approximately 7 deg, and the sweep angle Λ_c was found to be 76.5 deg. Far from the cores, the PDV-measured velocity approaches the empty-tunnel value.

A CFD solution using the Baldwin–Lomax closure model was obtained by Rizzetta[29] for a similar flowfield and is shown beneath each of the PDV images. The overall flow structure and the ranges of velocity found in the flow are in approximate agreement, but the vortex-core diameters measured by PDV are only one-third to one-half the value from the CFD solution. This may be due to insufficient

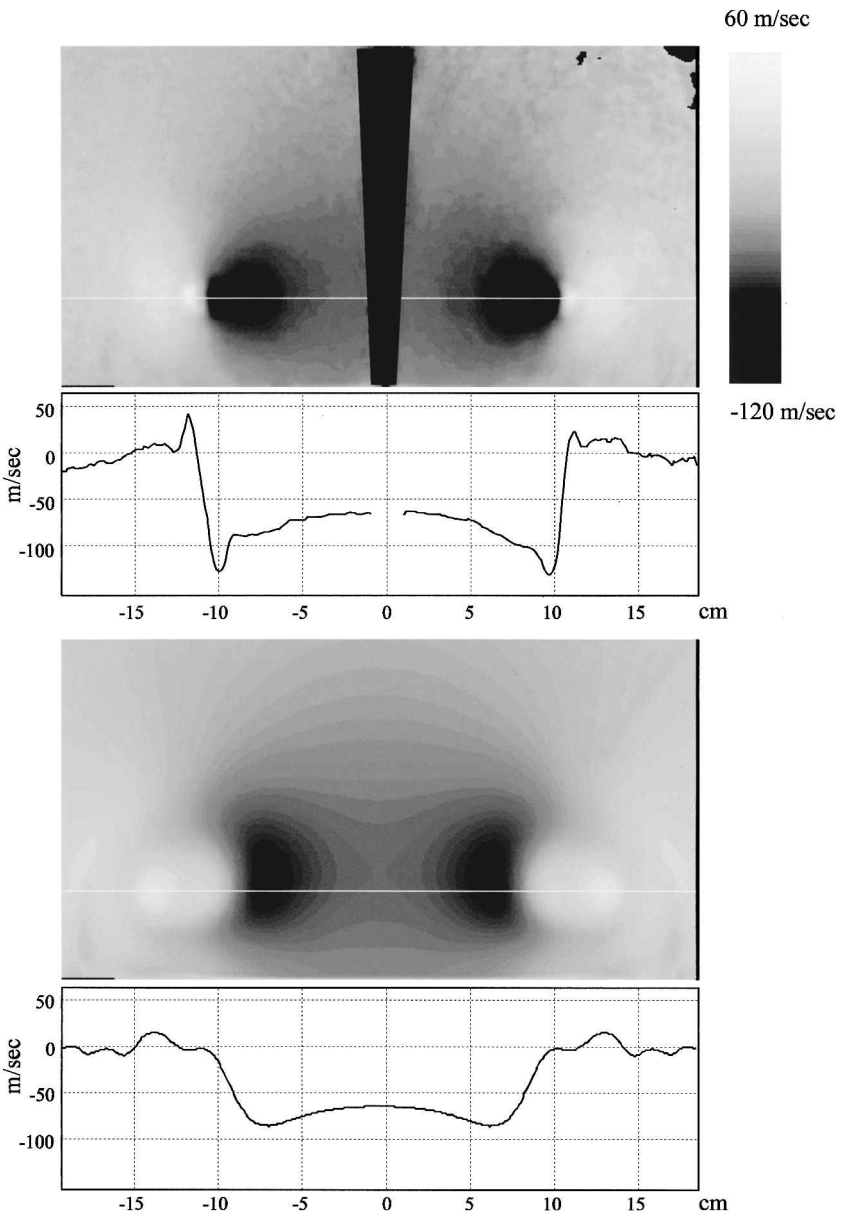

Fig. 9 Average PDV measurements of the flow over a delta wing at 103% root chord with comparison to the CFD simulation.[29]

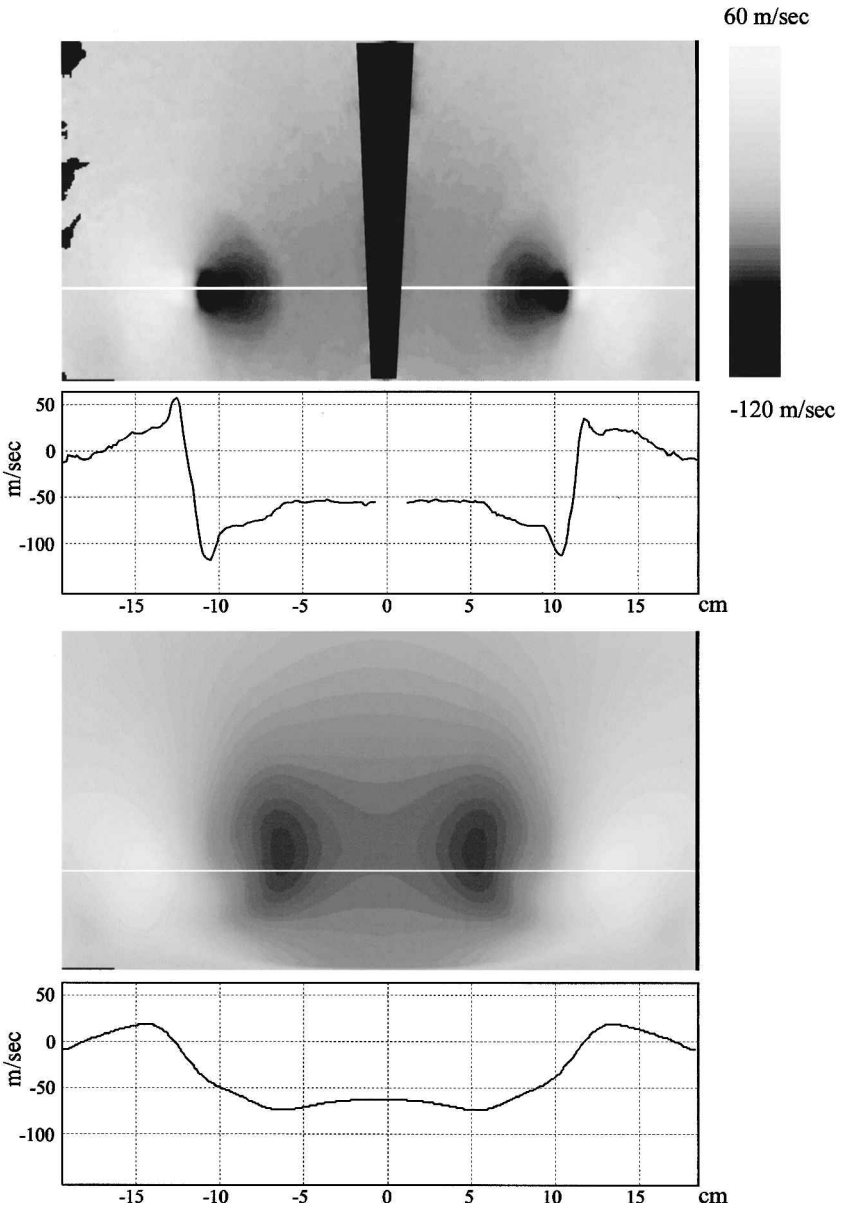

Fig. 10 Average PDV measurements of the flow over a delta wing at 114% root chord with comparison to the CFD simulation.[29]

grid resolution in the CFD solution or the choice of the turbulence model. Note, finally, that in both the PDV measurements and the CFD solution at 97% root chord, the free-shear layer can be observed rolling up from the leading edge of the wing at about ±15 cm.

Figure 11 shows average PDV images for the delta wing with tails; these measurements were based on 89, 45, 82, and 48 images for the respective locations of 86, 97, 103, and 114% root chord. Flow visualizations by Beutner et al.[30] indicated that vortex bursting occurred at approximately the midchord location on the wing and oscillated by ~5% chord in the streamwise direction. Thus, the measurement planes of the current experiment were downstream of the burst location. These images show a much more diffuse vortex structure, consistent with the phenomenon of vortex bursting. No comparison with CFD results is presented here because the CFD solution was not able to predict the burst location correctly. Note that a rather strong positive region in the measured velocity component exists on the inboard surface of the tails. This may indicate that the vortex has moved slightly inboard for the tails-on case or may result from the upstream flow in the vortex core past the burst point.

Error Analysis

Five principal sources of bias error were identified by an examination of Eq. (2); complete details of the analysis may be found in Ref. 28. Dominant contributions to the error include the uncertainty in ϕ and parameters contributing to uncertainty in ζ_c and ζ_r: the filter side-arm temperature, the baseline voltage of the gated integrators, and the scaling factor applied to the frequency functions.

The bias error associated with these sources for the case of the jet is given in Fig. 12a for the velocity range 100–280 m/s. The absolute error is approximately constant over the range of velocities investigated. The reason for this is that the dominant error terms are associated with the measurement of the laser set-point frequency, which itself is constant. The source of this uncertainty is due to the uncertainty in the factor used to scale the transmission of the frequency-monitoring system to unity. The bias error is given for the case of the wind tunnel in Fig. 12b over the velocity range −120–40 m/s. At the negative velocities, all error terms contribute comparably, but for positive velocities, the scaling error of the camera frequency function ζ_c is dominant.

The following mechanisms have been identified as sources of random error in the measurement of the transmission: the radiometric noise associated with the CCD cameras,[10] digital truncation errors associated with the gated integrators, laser speckle noise,[14,18] and a residual random error associated with frequency-monitoring system. Figure 13 shows the random error in velocity arising from the sources discussed for the jet and for the wind tunnel over a selected velocity range. Laser speckle is the dominant source of this random error.

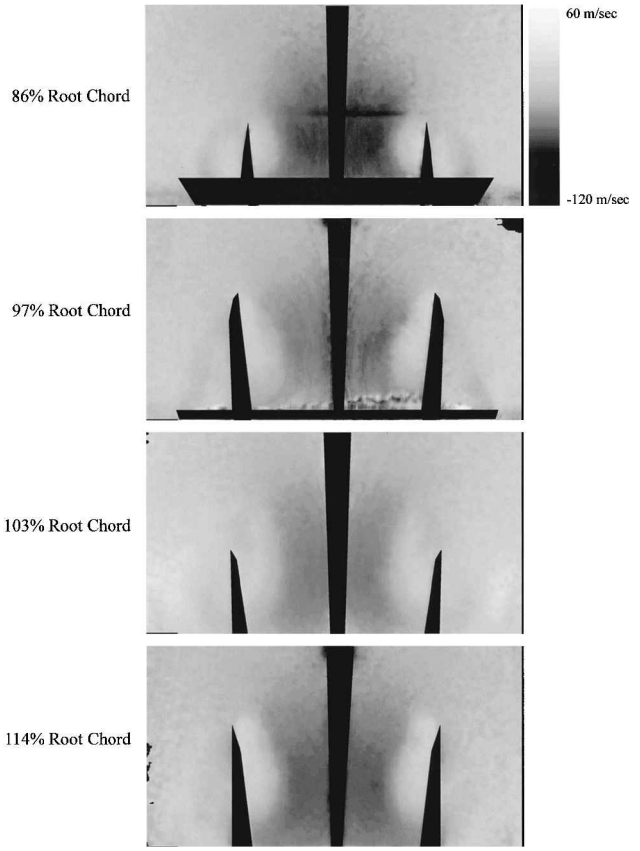

Fig. 11 Average PDV measurements of the flow over a delta wing with tails at four root-chord locations.

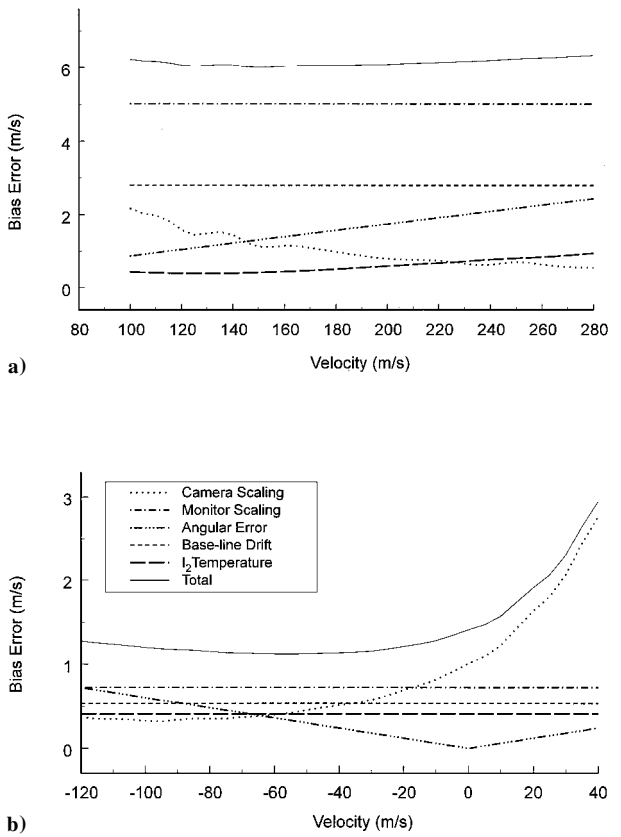

Fig. 12 Absolute bias error for a) jet and b) wind-tunnel experiments over a selected velocity range.

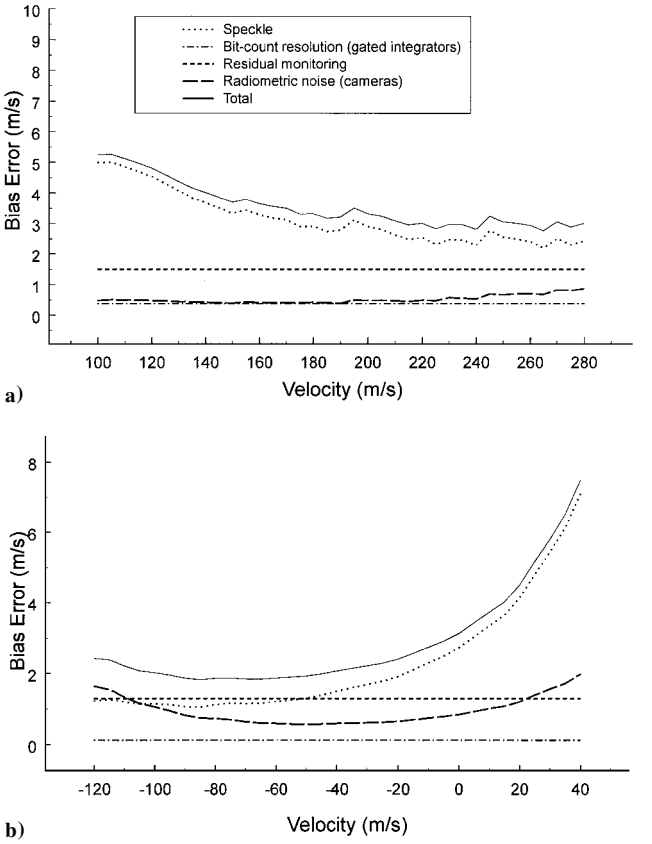

Fig. 13 Absolute random error for a) jet and b) wind-tunnel experiments over a selected velocity range.

Speckle noise is introduced when laser light is scattered off a surface or from a cloud of particles; small differences in path length of the scattered light cause three-dimensional interference patterns. If the speckle pattern in these image pairs were perfectly correlated, then the ratio step would remove the speckle noise. However, the signal and reference speckle patterns do not exhibit perfect correlation. Part of the reason for this is imperfect mapping; that is, corresponding pixels in the two images do not necessarily correspond to exactly the same flow regions (a problem that can be exacerbated by facility vibrations). Nonetheless, even with perfect mapping, minute differences in path length between the signal and reference images can degrade the correlation in speckle patterns because they are three dimensional.

Conclusions

The PDV technique has been described and demonstrated in small- and large-scale facilities. The system developed for these studies featured a laser-frequency-monitoring system that was capable of resolving the laser centerline frequency to better than 4 MHz on each laser pulse. Mean measurements in the core of the Mach 1.36 jet were within 2.4% (6.4 m/s) of the values obtained by LDV, and instantaneous velocity fluctuations were measurable to within about 3% (9 m/s) of the core velocity; improvements in this value would have been realized by using a faster lens aperture. In the wind tunnel, mean empty-tunnel measurements were within 2 m/s of the expected tunnel velocity, and instantaneous velocity fluctuations were within 4 m/s of the expected fluctuations. Remarkably, the frequency shift associated with these velocities is much smaller than the frequency width of the laser light. Mean measurements of the flow over a delta wing showed velocity ranges comparable to those from a CFD simulation, but indicated that the vortex-core diameters are somewhat smaller than predicted by the simulation. Measurements of the same delta-wing model equipped with vertical tails showed that the vortices become more diffuse, consistent with the phenomena of vortex bursting. The wind-tunnel measurements were performed in an environment that was challenging due to the scale of the facility, vibrations, and optical-access limitations.

Nonetheless, this study demonstrates the efficacy of PDV for wind-tunnel testing.

Acknowledgments

C. D. Carter was supported under U.S. Air Force Contracts F33615-97-C-2702 and F33615-97-C-3004. G. S. Elliott was supported by the National Science Foundation (CTS 97-33388), J. Foss, Program Manager. The authors would like to thank K. Kirkendall (Taitech, Inc.) for performing the laser Doppler velocimetry measurements, W. Weaver for writing the data collection programs, and D. Rizzetta for providing the computational fluid dynamics data presented.

References

[1]Drain, L., *The Laser Doppler Technique*, Wiley, New York, 1980.

[2]Shimizu, H., Lee, S., and She, C., "High Spectral Resolution Lidar System with Atomic Blocking Filters for Measuring Atmospheric Parameters," *Applied Optics*, Vol. 22, No. 9, 1983, pp. 1373–1381.

[3]Miles, R., Lempert, W., and Forkey, J., "Instantaneous Velocity Fields and Background Suppression by Filtered Rayleigh Scattering," AIAA Paper 91-0357, Jan. 1991.

[4]Komine, H., and Brosnan, S., "Instantaneous, Three-Component, Doppler Global Velocimetry," *Laser Anemometry*, Vol. 1, Aug. 1991, pp. 273–277.

[5]Meyers, J., and Komine, H., "Doppler Global Velocimetry: A New Way to Look at Velocity," *Laser Anemometry*, Vol. 1, Aug. 1991, pp. 289–296.

[6]Miles, R., Forkey, J., and Lempert, W., "Filtered Rayleigh Scattering Measurements in Supersonic/Hypersonic Facilities," AIAA Paper 92-3894, July 1992.

[7]Forkey, J., Finkelstein, N., Lempert, W., and Miles, R., "Control of Experimental Uncertainties in Filtered Rayleigh Scattering Measurements," AIAA Paper 95-0298, Jan. 1995.

[8]Forkey, J., Lempert, W., and Miles, R., "Observation of a 100-MHz Frequency Variation Across the Output of a Frequency-Doubled Injection-Seeded Unstable-Resonator Q-Switched Nd:YAG Laser," *Optics Letters*, Vol. 22, No. 4, 1997, pp. 230–232.

[9]Elliott, G., Samimy, M., and Arnette, S., "Details of a Molecular Filter-Based Velocimetry Technique," AIAA Paper 94-0490, Jan. 1994.

[10]McKenzie, R., "Measurement Capabilities of Planar Doppler Velocimety Using Pulsed Lasers," *Applied Optics*, Vol. 35, No. 6, 1996, pp. 948–964.

[11]Naylor, S., and Kuhlman, J., "Accuracy Studies of a Two-Component Doppler Global Velocimeter," AIAA Paper 97-0508, Jan. 1997.

[12]Clancy, P., Samimy, M., and Erskine, W., "Planar Doppler Velocimetry: Three-Component Velocimetry in Supersonic Jets," AIAA Paper 98-0506, Jan. 1998.

[13]Smith, M., "Application of a Planar Doppler Velocimetry System to a High Reynolds Number Compressible Jet," AIAA Paper 98-0428, Jan. 1998.

[14]McKenzie, R., "Planar Doppler Velocimetry Performance in Low-Speed Flows," AIAA Paper 97-0498, Jan. 1997.

[15]Clancy, P., and Samimy, M., "Two Component Planar Doppler Velocimetry in High Speed Flows," *AIAA Journal*, Vol. 35, No. 11, 1997, pp. 1729–1738.

[16]Smith, M., and Northam, G., "Application of Absorption Filter-Planar Doppler Velocimetry to Sonic and Supersonic Jets," AIAA Paper 0299, Jan. 1995.

[17]Smith, M., Northam, G., and Drummond, P., "Application of Absorption Filter Planar Velocimetry to Sonic and Supersonic Jets," *AIAA Journal*, Vol. 34, No. 3, 1996, pp. 434–441.

[18]Smith, M., "The Reduction of Laser Speckle Noise in Planar Doppler Velocimetry Systems," AIAA Paper 98-2607, June 1998.

[19]Arnette, S., Samimy, M., and Elliott, G., "Two Component Filtered Planar Velocimetry in the Compressible Turbulent Boundary Layer," AIAA Paper 96-0305, Jan. 1996.

[20]Meyers, J., Lee, J., and Cavone, A., "Three Component Doppler Global Velocimeter Measurements of the Flow Above a Delta-Wing," 6th International Symposium on Applications of Laser Techniques to Fluid Mechanics, Lisbon, July 1992.

[21]Meyers, J., Lee, J., Cavone, A., and Suzuki, K., "Investigation of the Vortical Flow Above an F/A-18 Using Doppler Global Velocimetry," American Society of Mechanical Engineers, Fifth International Conf. on Laser Anemometry, Aug. 1993.

[22]Beutner, T., Baust, H., and Meyers, J., "Doppler Global Velocimetry Measurements of a Vortex-Tail Interaction," *Proceedings of the 7th International Symposium on Flow Visualization*, Optical Diagnostics in Engineering, Seattle, WA, 1995.

[23]Meyers, J., "Evolution of Doppler Global Velocimetry Data Processing," 8th International Symposium on Applications of Laser Techniques to Fluid Mechanics, Lisbon, July 1996.

[24]Roehle, I., "Three Dimensional Doppler Global Velocimetry in the Flow of a Fuel Spray Nozzle and in the Wake Region of a Car," *Flow Measurement and Instrumentation*, Elsevier Science, New York, 1997, pp. 287–294.

[25]Arnette, S., Elliott, G., Mosedale, A., and Carter, C., "A Two-Color Approach to Planar Doppler Velocimetry," AIAA Paper 98-0507, Jan. 1998.

[26]Shirley, J., and Winter, M., "Air-Mass Flux Measurement System Using Doppler-Shifted Filtered Rayleigh Scattering," AIAA Paper 93-0513, Jan. 1993.

[27]Elliott, G., and Samimy, M., "A Molecular Filter Based Technique for Simultaneous Measurements of Velocity and Thermodynamic Properties," AIAA Paper 96-0304, Jan. 1996.

[28]Mosedale, A., "An Investigation of the Planar Doppler Velocimetry Technique," M.S. Thesis, Dept. of Mechanical and Aerospace Engineering, Rutgers Univ., New Brunswick, NJ, Oct. 1998.

[29]Rizzetta, D., "Numerical Simulations of the Interaction Between a Leading-Edge Vortex and a Vertical Tail," AIAA Paper 96-2012, 1996.

[30]Beutner, T., Elliott, G., Mosedale, A., and Carter, C., "Doppler Global Velocimetry Applications in Large-Scale Facilities," AIAA Paper 98-2608, June 1998.

[31]Visbal, M., "Computational and Physical Aspects of Vortex Breakdown on Delta-Wings," AIAA Paper 95-0585, Jan. 1995.

M. Samimy
Associate Editor